Ternary systems based on ZnO/CeO2/Cu2O for the degradation of phenol and carbamazepine

Ternary systems based on $ZnO/CeO_2/Cu_2O$ for the degradation of phenol and carbamazepine

Erik Cerrato, Elettra Rebolini, Debora Fabbri, Paola Calza, Maria Cristina Paganini*

Dipartimento di Chimica e Centro NIS, Via Giuria 7, 10125, Torino

Email corresponding author : mariacristina.paganini@unito.it

Key words: ZnO mixed system, CeO_2, Cu_2O, hydrothermal synthesis, organic pollutants degradation

Abstract

In this paper we prepared via different synthetic processes, two ternary systems based on ZnO, CeO_2 and Cu_2O for the abatement of organic pollutants. The system ZnO/CeO_2 was already known to be efficient in the degradation of emergent contaminants, the addition of cuprous oxides allows also to enhance reductive properties to the material thanks to its specific potential. The mixed oxides were characterized via power X Ray Diffraction, UV visible Diffuse Reflectance and Electron Paramagnetic Resonance. The materials obtained through hydrothermal synthesis shown better performances in the abatement of phenol and carbamazepine.

1. Introduction

The search for new materials that work as photocatalysts is constantly evolving. In recent years, much attention has been paid to various methods for modifying the classic first generation semiconductors such as TiO_2. Among the different types of material engineering, the most used are the intrinsic and extrinsic doping, the formation of solid solutions and the creation of heterojunctions at the interface between two materials that have no tendency to form solid solutions. The development of semiconductor-semiconductor composite heterojunctions for efficient photocatalytic pollutant degradation is of great interest. ZnO is one of the most abundant, cheap and non-toxic semiconductor, already employed for degradation of different pollutants [1-3].

The photocatalytic degradation process depends on various factors: the light-absorption ability of the semiconductor, which in turn depends on its surface area and morphology, optical band gap and in particular the charge separation capability [4]. The photocatalytic performances of ZnO can be improved either through doping with metals or nonmetals or via the preparation of ZnO heterostructures with other semiconductor elements [5]. Composite nanostructures of transition metal oxides are of great interest because of their tunable optical as well as catalytic properties.

Recently, our and other [6-8] research groups started to investigate the role of cerium as dopant of oxides. In our approach, cerium ions are not soluble in the ZnO matrix. This composite system has shown an amazing, unexpected activity in the mineralization of acesulfame K, a so-called emerging pollutant, performed under visible light [9]. This result led us to an in-depth study of this new material. We observed that the CeO_2/ZnO system is biphasic and the role of the solid−solid interface plays a crucial role in the photo-activity of the material.

Coupled semiconductors formed by ZnO and other metal oxides or sulfides (e.g., CuO, Cu_2O, CdO, CuS, CdS, and ZnS) have been employed as photocatalysts, enhancing the charge carrier separation ability (electrons and holes) between adjacent semiconductors [10]. In particular, cupric and cuprous oxides (CuO and Cu_2O) are nontoxic p-type metal oxide semiconductor having an optical band gap in the range from 1.2 to 2.2 eV [11]. Moreover, Cu_2O is considered very interesting thanks to its relative band position with respect to the normal hydrogen electrode (NHE) (- 1.2 eV for the conduction band and +1.3 eV for the valence band). It has been demonstrated that it instigates reduction and oxidation of different pollutants via the formation of hydroxyl and superoxide radicals (with formation energies of approximately +1.23 and - 0.28 eV, respectively), which are the main reactive species in photocatalytic reactions [12]. Accordingly, addition of Cu_2O to ZnO in a ZnO–Cu_2O–CuO nanocomposite configuration could result in photocatalytic activity superior to that of the intrinsic ZnO semiconductor system. As it will be shown below, it is indeed the role of these interfaces (or heterojunctions) that allows a better understanding of this novel promising photocatalytic system. In the present work we prepared nanocomposite systems coupling CeO_2/ZnO materials with Cu_2O particle with two different synthetic methods. The preparation process influences the surface area and the crystallinity of the photocatalysts affecting also their photocatalytic properties. We tested these materials in the degradation of a classic probe molecule like phenol and of an emergent pollutant such as carbamazepine.

2. Experimental section

All reactants employed were purchased by Sigma-Aldrich and used without any further purification treatment. Distilled water was used in the synthesis procedures. Synthesis procedure will be described for each system in the following corresponding section.

The investigated samples were mainly prepared via hydrothermal and precipitation synthetic routes, described hereafter.

2.1 Hydrothermal synthesis.

Pristine ZnO and ZnO containing 1% molar of cerium were prepared by means the hydrothermal method and they were labelled ZnO-H, CZ1-H, respectively. The bare sample were synthetized preparing a solution 1M of $Zn(CH_3COO)_2 \cdot 2H_2O$ in 20 ml of H_2O. Subsequently, NaOH 4M was added to the solution until to reach a pH value of 11. The obtained solution was transferred into a PTFE-lined stainless steel 100 mL autoclave and heat at 448 K for 12 hours. The product was centrifuged, washed three times with distilled water and dried at 343 K overnight. The mixed sample CZ1-H was synthetized adding to the starting solution the corresponding stoichiometric amount of $CeCl_3*7H_2O$.

2.2 Precipitation synthesis.

Even with this synthetic approach a bare sample of ZnO and a sample containing 1% of Ce were prepared, labelled as ZnO-P and CZ1-P, respectively. The synthesis of the pristine material provides the dissolution of 2.2 g of $Zn(CH_3COO)_2*2H_2O$ in 160 mL of H_2O and 80 mL of EtOH; the formed solution is left in stirring for 1 h and subsequently 120 mL of NaOH 1M were added. The precipitated, after 48 h, was separated via filtration, washed with H_2O and dried at 343 K for 12 h. the final product was obtained after calcination at 573 K in air for 30 h. The mixed sample CZ1-P, containing 1% molar of Ce, was synthetized adding the corresponding stoichiometric amount of $CeCl_3*7H_2O$ to the starting mixture.

2.3 Cupper modified oxide systems.

Cu_2O-ZnO-P, Cu_2O-CZ1-P and Cu_2O-ZnO-H Cu_2O-CZ1-H were prepared by chemical reduction followed by deposition method. At 10 mL of $Cu(NO_3)_2*3H_2O$ $7.9*10^{-3}$ M (0.5% wt on the basis of the oxide) water solution were added 0.0568 g of glucose and 15 mL of NaOH $2.36*10^{-3}$ M. The solution was stirred for 50 min at 343 K. At the end of the reaction an orange suspension was formed (indicated as suspension A). In this reaction, known as Benedict reaction[13], glucose reduces Cu^{2+} to Cu^{+} allowing the formation of Cu_2O oxide. 1 g of oxide was added in 20 mL of deionized water and the suspension was sonicated at 333 K for 10 min (indicated as suspension B). The suspension B was added to the suspension A and stirred for 10 min at 343 K. After this time the obtained orange powder was filtered and washed three times with water and ethanol, in order to remove the reaction residues and finally dried at 343 K.

2.4 X-Ray Powder Diffraction

Powder X-ray diffraction (XRD) patterns were recorded with a PANalytical PW3040/60 X'Pert PRO MPD diffractometer using a copper K_α radiation source (0.154056 nm). The intensities were

obtained in the 2θ range between 20° and 80°. X'Pert High-Source software was used for data handling.

2.5 UV Visible Diffuse Reflectance Spectroscopy (DRS)

UV-Visible absorption spectra were recorded using a Varian Cary 5 spectrometer, coupled with an integration sphere for diffuse reflectance acquisition, using a Carywin-UV/scan software. A sample of PTFE with 100% reflectance was employed as the reference. Spectra were registered in the 200-800 nm range at a scan rate of 240 nm/min with a step size of 1 nm. The measured intensities were converted with the Kubelka-Munk function.

The optical band gap energies were calculated considering that the energy dependence of the absorption coefficient (α) for semiconductors in the region near the absorption edge is given by:

$$\alpha \propto \frac{(hv - E_{bg})^{\eta}}{hv}$$

Where hv is the energy of the incident photon and E_{bg} is the optical absorption energy. η depends on the type of optical transition and since ZnO shows a direct-allowed optical transition its value is of 1/2. Finally, since the scattering coefficient weakly depends on energy and $F(R_\infty)$, it can be assumed as proportional to the absorption coefficient within the narrow range of energy containing the absorption edge feature.

$$F(R_\infty) = \frac{(hv - E_{bg})^{\eta}}{hv}$$

Then, the plot $(F(R_\infty)*hv)^{1/\eta}$ vs hv can be used to determine the absorption edge energy (Tauc plot) method[14].

The UV-Visible DRS studies after irradiation of the copper oxide impregnated samples were performed irradiating 0.4 g of samples suspended in 2 ml of water/ethanol solution (10% v/v) in a quartz cell for DRS measurements. After irradiation, prior to spectra acquisition the sample were let to sediment on the bottom of the DRS cell. The UV-Visible DRS spectra were recorded in the 200-800 nm range at a scan rate of 240 nm/min with a step size of 1 nm. Since during the irradiation was not possible to stir the samples, after every irradiation the samples were sonicated in order to homogenize the powders.

2.6 BET surface area

123 The specific surface area measurements were carried out on a Micrometrics ASAP 2020 using the
124 Brunauer-Emmett-Teller (BET) model on the N_2 adsorption measurement. Prior to the adsorption
125 run, all the samples were outgassed at 573K for 2h.
126 *2.7 EPR*
127 Electron Paramagnetic Resonance (EPR) spectra were recorded at room temperature and at
128 liquid nitrogen temperature (77 K). They were run on a X-band CW-EPR Bruker EMX spectrometer
129 equipped with a cylindrical cavity operating at 100 kHz field modulation.
130 *2.8 Photacatalytic tests*
131 The irradiation experiments were carried out in closed Pyrex cells (40 mm id x 25mm) on 5 mL of
132 suspension in Milli-Q water containing 1 g/L of catalyst and 20 mg/L of compound kept under
133 continuous stirring. The samples were irradiated using a Philips TLK 05 Blacklight lamp (40 W) with
134 a maximum emission of 365 nm. The suspensions were then filtered with Millipore 0.45 µM Millex
135 LCR hydrophilic PTFE filters and analysed via HPLC-UV.
136 The analyses for carbamazepine and phenol were carried out with a Merck-Hitachi HPLC system
137 equipped with a L-6200A Intelligent Pump, a L-4200 UV-VIS Detector and a six-way Rheodyne valve
138 injection system. Isocratic elution was performed with a mixture of phosphoric acid solution at pH
139 2.8 and acetonitrile at a flow rate of 1 ml/min. Condition are as follows: 60/40 and 70/30 v/v with
140 retention times of 3.77 and 4.83 min for carbamazepine and phenol, respectively. Detection
141 wavelength were 285 for carbamazepine and 220 nm phenol.
142
143 ## *3. Results and discussion*
144 *3.1 Structural and optical characterization*
145 The ZnO nanoparticles synthetized via precipitation and hydrothermal methods were analysed
146 from a structural point of view by means of X-ray powder diffraction. The structural analysis of these
147 materials has been already well described elsewhere [2, 15], the diffrattograms have been reported in
148 the supporting information section (see figure S1), showing the typical pattern of ZnO wurtzitic
149 hexagonal phase (00-036-1451 ICDD pattern) [16].
150 The optical properties of the synthetized samples were investigated by UV-Vis diffuse reflectance
151 spectroscopy; in Fig. S2 the reflectance measurements and the derived absorbance, obtained by the
152 application of the Kubelka-Munk equation, are reported. The reflectance and absorbance spectra
153 of CZ1 are dominated by the valence band (VB) – conduction band (CB) transition of ZnO, as already
154 explained in previous paper [2, 15].

Figure 1 panel A reports the XRD patterns of the bare ZnO-P and of the mixed system CZ1-P following the impregnation of 0.5 % of Cu_2O, occurring through the reaction described in the experimental section, named ZnO-Cu_2O-P and CZ1-Cu_2O-P, respectively. Figure 1 panel B reports the XRD diffraction patterns of the sample prepared via hydrothermal way. As in the cases reported in the SI section, the impregnated bare oxide shows the pattern typical of the wurtzitic hexagonal phase and no additional reflections due to impurities or to the cubic Cu_2O lattice were detected. The same diffraction pattern has been also registered for CZ1-Cu_2O-P, with the unique difference that in this case a slightly and very weak reflection is present around 2θ = 28.6°, due to the presence of CeO_2 phase.

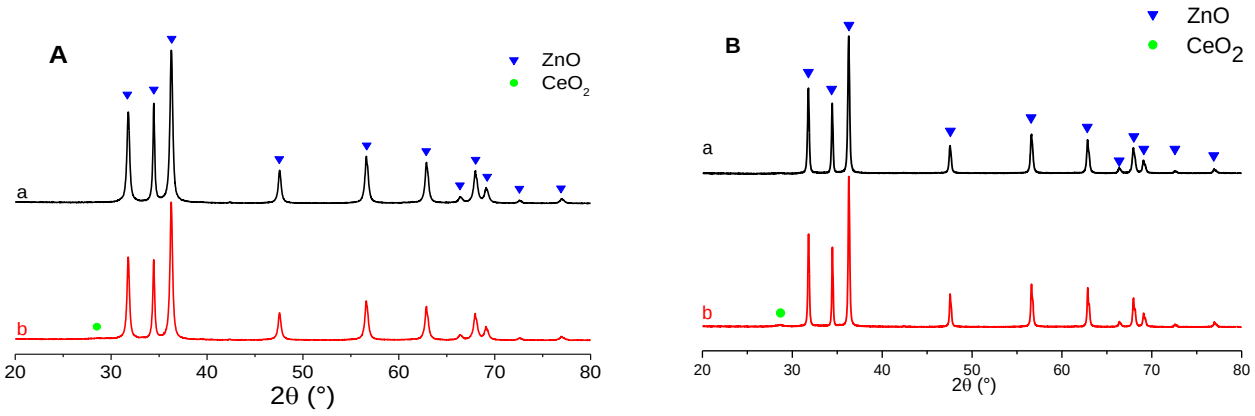

Figure. 1. *XRD patterns of the synthetized materials. Panel A: a) ZnO-Cu_2O-P and b) CZ1-Cu_2O-P. Panel B: a) ZnO-Cu_2O-H and b) CZ1-Cu_2O-H The green dot evidences a weak diffraction peak due to CeO_2.*

Then, XRD analysis was not able to detect the fingerprints of the Cu_2O crystal structure, probably because of the too lower concentration of copper compounds (0.5 %) and characterized by very small size. In addition, the most intense reflections should be at 2θ angles around 30° and 40°, where the intense reflections of the ZnO phase are already present.

Nevertheless, XRD analysis didn't evidence the presence of copper(II) oxide, the occurred impregnation was guaranteed by a net visible pink/orange color hired by the previously white samples (ZnO-P, ZnO-H and CZ1-P, CZ1-H).

We already described elsewhere [15] that the presence of cerium oxide has been demonstrated both via XRD measurements and also via TEM images where it is clear that the crystals of CeO_2 are much smaller that the ZnO ones. Also the measure of the surface area of the non –impregnated materials have been already reported. In the case of impregnated materials, we observed that the presence of copper oxide does not affect the surface area that remains identical to the samples without impregnation. The surface area for the pure ZnO samples (impregnated and non-

impregnated with copper) obtained via precipitation process or hydrothermal synthesis are 20 m^2/g and less than 10 m^2/g respectively, while the mixed samples CZ1 (impregnated and non-impregnated with copper) obtained via precipitation process or hydrothermal synthesis are 31 m^2/g and less than 10 m^2/g, respectively. Again precipitation synthesis process leads to the formation of samples with higher surface area.

In this sense, DR UV-vis spectroscopy gave a clear outcome, as reported in Figure 2, where the presence of Cu_2O can be deduced.

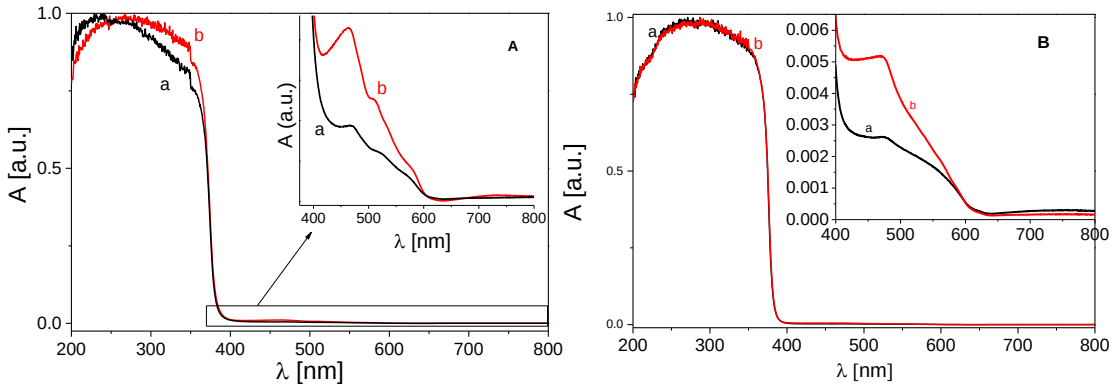

Figure. 2. *Normalized Absorbance Kubelka-Munk transformed diffuse reflectance spectra. Panel A: a) ZnO-Cu_2O-P and b) CZ1-Cu_2O-P; panel B: a) ZnO-Cu_2O-H and b) CZ1-Cu_2O-H*

Indeed, the spectra for the modified samples show, beside the band gap transition in the UV region, due to the excitation of electrons from the valence band to the conduction band [17], further absorptions in the visible region. The zoom evidences the presence of absorption bands in the range of wavelength between 400-600 nm, typical of Cu_2O particles [18-21]. More in details, the shoulder around 460 nm is suggested to derive by the interface charge transfer from the VB of ZnO to the Cu^{2+} that may also cause a partial reduction of the copper species. The second well recognizable band around 520 nm is due to the electronic transition from the valence band to the conduction typical of Cu_2O, showing a band gap width of 2.39 eV [19]. Less visible is the broad absorption between 600-800 nm, witnessing the presence of Cu(II) species, and in particular related to d-d transitions: this seems suggest that, beside Cu_2O nanoparticles, also a small fraction of Cu(II) is present in the impregnated samples.

Definitely, the presence of the impregnating Cu_2O phase greatly modify the optical behavior of the two different samples (P and H), particularly inducing absorption in the visible range, not previously detected for the not impregnated samples.

Finally, none appreciable red-shift in the energy gap of ZnO has been observed, suggesting that the Cu incorporation inside the matrix has been not occurred, but the Cu_2O particles are adsorbed at the surface of ZnO.

3.2 EPR characterization of the Cu_2O impregnated materials

The presence of the Cu^{2+} species has been also confirmed performing EPR spectra of the impregnated ZnO-Cu_2O and CZ1-Cu_2O samples. Indeed, Cu^{2+} ions ($3d^9$) show one unpaired electrons, differently from the diamagnetic Cu^+ and Cu^0, characterized by distinguishable fingerprint. The signal exhibits an axial *g* tensor splitted in four hyperfine lines since the Cu nucleus has a nuclear spin I = 3/2 and the derived line multiplicity is *n* = 2I+1= 4, so four lines are expected.

Both EPR spectra of the two materials, represented in Figure 3, are dominated by the typical axial signal of Cu^{2+}; in addition, the signal always visible in ZnO around *g* = 1.96 and attributed to electrons trapped in shallow donors [4], is also recorded. The signal at g = 1.96 is more likely associated to electrons in the conduction band or in a band built up by donor levels just below the bottom of the conduction band [2, 22-24]. This indicates that some (paramagnetic) defects, related to the matrix are always present but their concentration is strictly dependent on the synthesis procedure. In the case of precipitation process the intensity of this signal is much lower respect to that obtained for the sample prepared via hydrothermal synthesis; most probably this difference in intrinsic defectivity will affect the photocatalytic properties of the materials, as it will be demonstrated later.

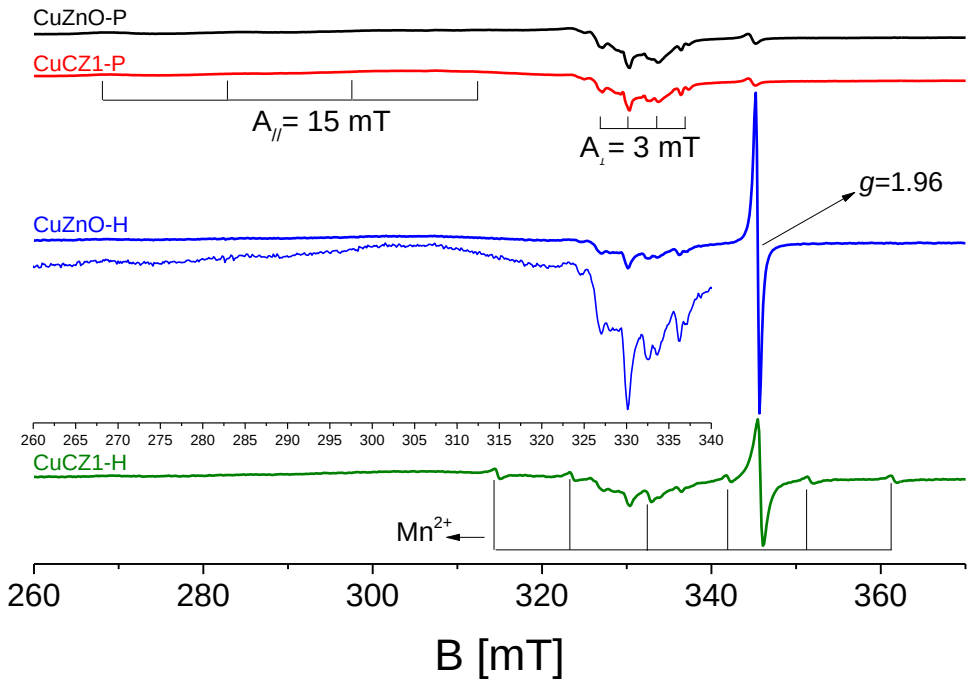

Figure. 3. *EPR spectra at 77K of ZnO-Cu_2O-P (black line), CZ1-Cu_2O-P (red line) ZnO-Cu_2O-H (blue line) and CZ1-CU_2O-H (green line).*

In Figure 3 it is possible to observe that the hyperfine structure results slightly visible in the parallel component while it is better resolved in the perpendicular one. The signal features are $A_{//}$ = 15 mT and $A_{\perp}$ = 3.1 mT where *A* is the hyperfine tensor: the fact that both the parallel and the perpendicular hyperfine structure are observable has been ascribed as isolated Cu(II) ions, that in our case come as synthetic "waste", caused by unavoidably oxidation during the synthesis procedure. Another confirmation that the Cu^{2+} ions are not embedded inside ZnO or CeO_2 lattices is represented by the fact that for this situation the *A* values reported would be smaller than in our case [25-28].

Thus, combining DR-UV-vis and EPR spectroscopy the samples impregnated with copper(I) oxide exhibit, in addition to small Cu_2O particles (not visible with XRD but certified by DR UV-vis) anchored to oxide surfaces, a certain amount of Cu(II), dispersed on the surface of the two materials.

3.3 Photocatalytic efficiency of the developed materials

The efficiency of the developed materials was tested toward the abatement of two molecules: carbamazepine (CBZ) and phenol (PHE). Preliminarily, adsorption in the dark was performed with all materials toward the two analytes and was negligible. A contribution of direct photolysis in the considered time window (2h) can be excluded as well.

3.3.1 Photocatalysts synthetized via precipitation

The degradation profiles obtained for the two investigated molecules in the presence of the developed photocatalysts are plotted in Figure 4; the degradation achieved in the presence of the benchmark TiO_2 P25 is reported as well for comparison purpose. In all cases, the degradation process approximates a pseudo first order kinetic and the calculated constants are collected on Table 1.

Considering the case of samples P shown in Figure 4 A, P25 and pristine ZnO exhibit the lowest photoactivity and the changes introduced to the ZnO matrix by the presence of Cu_2O clearly increase the performance of the materials. In fact, even if the single heterojunction with cerium (CZ1) leads to a slight increase in the photocatalytic performance, copper single (Cu_2O-ZnO) and double (Cu_2O-CZ1) heterojunction prompted a faster degradation. This suggests that impregnation with Cu(I) may increase the charge separation produced within the material and the mobility of the charge carriers in the system with heterojunction.

In the case of CBZ, we observed the same trend for ZnO-based materials, and modifications with Cu(I) and Ce(IV) oxides favor the photocatalytic activity of the materials. However, the performance for all the precipitates are worse than P25 as perceived in Figure 4 B.

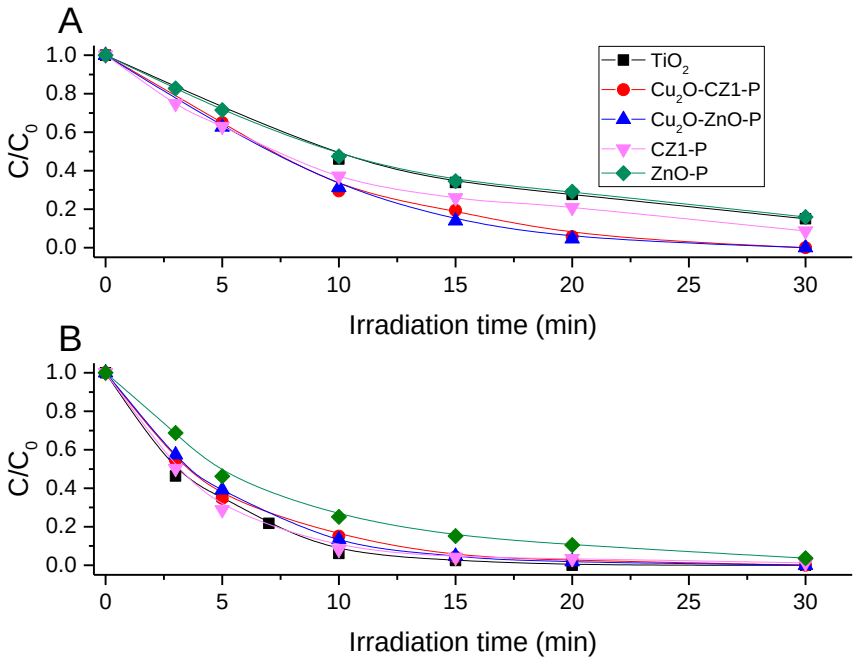

Figure 4. Degradation of phenol (A), carbamazepine (B) in the presence of photocatalysts prepared with precipitation method

3.3.2 Photocatalysts synthetized via hydrothermal method

We noticed that all ZnO-based materials exhibit a higher efficiency than P25 toward all the tested molecules as reported in Table 1.

Table 1. Kinetic constants for synthetized materials

K, min^{-1}	**TiO_2**	**ZnO-P**	**CZ1-P**	**Cu_2O-CZ1-P**	**Cu_2O-ZnO-P**	**ZnO-H**	**CZ1-H**	**Cu_2O-CZ1-H**	**Cu_2O-ZnO-H**
Phenol	0.061	0.060	0.080	0.139	0.153	0.104	0.340	0.478	0.327
Carbamazepine	0.257	0.108	0.145	0.189	0.203	0.252	0.873	1.249	0.256

Hydrothermal synthesis appears to be the optimal strategy for increasing the efficiency of the heterojunctions that form in the modified ZnO matrix. In fact, as it can be seen from the degradation curves in Figure 5, the system with single heterojunction between ceria and ZnO (CZ1) shows an improved performance compared to the same material produced by precipitation, while the double heterojunction composite (Cu_2O-CZ1) is the most active towards phenol. The positive role played by copper is confirmed with these experiments but, in this case, the synthesis strategy adopted seems

to optimize the synergistic effect of the two heterojunctions in promoting the mobility of the charge carriers, with a positive effect on the degradation of the target molecule.

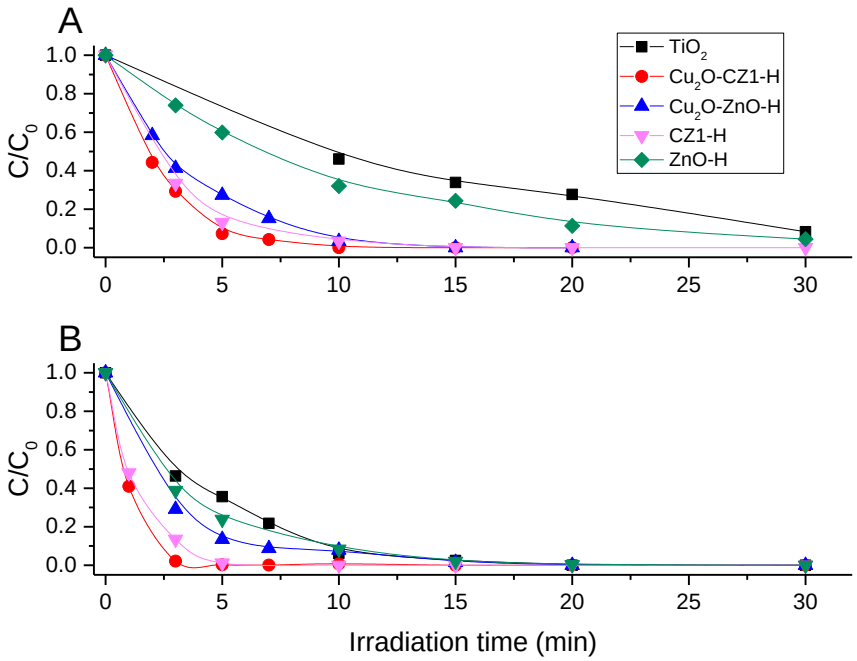

Figure 5. Degradation of phenol (A), carbamazepine (B) in the presence of photocatalysts prepared with hydrothermal method.

Analyzing more in detail samples P and H and comparing with the kinetic constants obtained for the different materials with the two different synthesis strategies, the choice of hydrothermal method seems decisive for the performance of the catalysts. The Cu_2O-CZ1-H system proves to be the most effective for the removal of this molecule from the aqueous medium, as depicted in Figure 5. In fact, the constants obtained with the hydrothermal materials are significantly higher than those calculated for the precipitated materials (0.34 min^{-1} for CZ1-H vs 0.08 min^{-1} for CZ1-P, 0.11 min^{-1} for ZnO-H vs 0.06 min^{-1} for ZnO-P, 0.48 min^{-1} for Cu_2O-CZ1-H vs 0.14 min^{-1} for the precipitate and 0.38 min^{-1} for Cu_2O-ZnO-H vs 0.15 min^{-1} for the precipitate). These results may be linked to the crystallinity of the samples obtained with the two synthesis methods; with hydrothermal method, a higher crystallinity is observed allowing a better and selective contact surface between the catalyst and the adsorbate, so favouring the oxidation-reduction reactions occurring among the charge carriers, the hydroxyl radicals and the pollutants.

Also for CBZ the hydrothermal synthesis has led to a higher degradation efficiency, as clearly shown in Figure 5 B. The activity shown by the CeO_2/ZnO system towards CBZ further supports that the addition of ceria and the formation of the heterojunction could allow charge separation and

electron stabilization in the f orbitals of Ce^{4+}. Moreover, thanks to the results obtained with the double heterojunction composite system (Cu_2O-CZ1), the synergistic effect of the double heterojunction seems to be confirmed; for it the calculated kinetic constant is 1.25 min^{-1}, the highest observed, and is five times higher than pristine ZnO-H (0.25 min^{-1}).

The type of synthesis method plays an important role in determining the efficiency for the abatement of the target molecules. In particular, hydrothermal materials are able to reduce 70 to 90% of the initial concentration of carbamazepine and phenol within five minutes of irradiation. The effectiveness of materials obtained by precipitation is always less than that of materials obtained by hydrothermal means. In fact, by comparing the kinetic constants, it comes up that the materials produced by precipitation have a lower performance than the materials synthesized by hydrothermal method. The employment of a double heterojunction $Cu_2O/ZnO/CeO_2$ seems the most promising in degrading phenol and carbamazepine. The role of the synthesis way seems to be crucial. It comes out also from the spectroscopic characterization that the two materials are different.

4. Conclusions

The formation of heterojunction between ZnO and CeO_2 has been observed experimentally in the past, the addition of Cu_2O nanoparticles on the surface of the mixed systems leads to the formation of a very active material in the abatement of phenol and carbamazepine molecules. Residual traces of Copper (II) not reduced have been evidenced by UV Vis analysis and EPR measurements. These species seem to be well dispersed over the surface of the semiconductors. The role of these species in the photo degradation process has still to be clarified. Moreover, also the photoacitivity under visible light is an interesting point that should be took in consideration in the next future. From these preliminary results we underlined the crucial role of the synthesis method in obtaining asuitable material for pollutants degradation.

Acknowledgment

Financial support from the Italian MIUR through the PRIN Project 20179337R7, MULTI-e "Multielectron transfer for the conversion of small molecules: an enabling technology for the chemical use of renewable energy" and the European Union's Horizon 2020 research and innovation programme under the Marie Skłodowska-Curie Grant Agreement No 765860 (AQUAlity) is gratefully acknowledge-edged.

339

1. Paganini, M. C.; Dalmasso, D.; Gionco, C.; Polliotto, V.; Mantilleri, L.; Calza, P., Beyond TiO2: Cerium-Doped Zinc Oxide as a New Photocatalyst for the Photodegradation of Persistent Pollutants. *ChemistrySelect* **2016,** *1* (12), 3377-3383.
2. Cerrato, E.; Gionco, C.; Paganini, M. C.; Giamello, E.; Albanese, E.; Pacchioni, G., Origin of Visible Light Photoactivity of the CeO2/ZnO Heterojunction. *ACS Applied Energy Materials* **2018,** *1* (8), 4247-4260.
3. Kodera, M.; Wang, J.; Nail, B. A.; Liu, J.; Urabe, H.; Hisatomi, T.; Katayama, M.; Minegishi, T.; Osterloh, F. E.; Domen, K., Investigation of charge separation in particulate oxysulfide and oxynitride photoelectrodes by surface photovoltage spectroscopy. *Chemical Physics Letters* **2017,** *683*, 140-144.
4. Yang, S.; Wang, L. J.; Yan, Y. S.; Yang, L. L.; Li, X.; Lu, Z. Y.; Zhai, H. J.; Han, D. L.; Huo, P. W., Two Hybrid Au-ZnO Heterostructures with Different Hierarchical Structures: Towards Highly Efficient Photocatalysts. *Scientific Reports* **2019,** *9*.
5. Saravanan, R.; Shankar, H.; Prakash, T.; Narayanan, V.; Stephen, A., ZnO/CdO composite nanorods for photocatalytic degradation of methylene blue under visible light. *Materials Chemistry and Physics* **2011,** *125* (1-2), 277-280.
6. Gionco, C.; Paganini, M. C.; Giamello, E.; Burgess, R.; Di Valentin, C.; Pacchioni, G., Cerium-Doped Zirconium Dioxide, a Visible-Light-Sensitive Photoactive Material of Third Generation. *Journal of Physical Chemistry Letters* **2014,** *5* (3), 447-451.
7. Bechambi, O.; Jlaiel, L.; Najjar, W.; Sayadi, S., Photocatalytic degradation of bisphenol A in the presence of Ce–ZnO: Evolution of kinetics, toxicity and photodegradation mechanism. *Materials Chemistry and Physics* **2016,** *173*, 95-105.
8. Bechambi, O.; Touati, A.; Sayadi, S.; Najjar, W., Effect of cerium doping on the textural, structural and optical properties of zinc oxide: Role of cerium and hydrogen peroxide to enhance the photocatalytic degradation of endocrine disrupting compounds. *Materials Science in Semiconductor Processing* **2015,** *39*, 807-816.
9. Calza, P.; Gionco, C.; Giletta, M.; Kalaboka, M.; Sakkas, V. A.; Albanis, T.; Paganini, M. C., Assessment of the abatement of acelsulfame K using cerium doped ZnO as photocatalyst. *J Hazard Mater* **2017,** *323* (Pt A), 471-477.
10. Madhusudan, P.; Wang, Y.; Chandrashekar, B. N.; Wang, W. J.; Wang, J. W.; Miao, J.; Shi, R.; Liang, Y. X.; Mi, G. J.; Cheng, C., Nature inspired ZnO/ZnS nanobranch-like composites, decorated with Cu(OH)(2) clusters for enhanced visible-light photocatalytic hydrogen evolution. *Applied Catalysis B-Environmental* **2019,** *253*, 379-390.
11. Harish, S.; Archana, J.; Sabarinathan, M.; Navaneethan, M.; Nisha, K. D.; Ponnusamy, S.; Muthamizhchelvan, C.; Ikeda, H.; Aswal, D. K.; Hayakawa, Y., Controlled structural and compositional characteristic of visible light active ZnO/CuO photocatalyst for the degradation of organic pollutant. *Applied Surface Science* **2017,** *418*, 103-112.
12. Basnet, P.; Zhao, Y. P., Tuning the CuxO nanorod composition for efficient visible light induced photocatalysis. *Catalysis Science & Technology* **2016,** *6* (7), 2228-2238.
13. Markina, N. E.; Pozharov, M. V.; Markin, A. V., Synthesis of Copper(I) Oxide Particles with Variable Color: Demonstrating Size-Dependent Optical Properties for High School Students. *Journal of Chemical Education* **2016,** *93* (4), 704-707.
14. Martra, G.; Gianotti, E.; Coluccia, S., The Application of UV - Visible - NIR Spectroscopy to Oxides. In *Metal Oxide Catalysis*, Jackson, S. D.; Hargreaves, J. S. J., Eds. WILEY-VCH Verlag GmbH & Co. KGaA, Weinheim: 2009; pp 51-94.
15. Cerrato, E.; Gionco, C.; Paganini, M. C.; Giamello, E., Photoactivity properties of ZnO doped with cerium ions: an EPR study. *J Phys Condens Matter* **2017,** *29* (44), 444001.
16. Özgür, Ü.; Alivov, Y. I.; Liu, C.; Teke, A.; Reshchikov, M. A.; Doğan, S.; Avrutin, V.; Cho, S. J.; Morkoç, H., A comprehensive review of ZnO materials and devices. *Journal of Applied Physics* **2005,** *98* (4), 041301.
17. Janotti, A.; Van de Walle, C. G., Absolute deformation potentials and band alignment of wurtzite ZnO, MgO, and CdO. *Physical Review B* **2007,** *75* (12).
18. Banerjee, S., Optical Absorption by Nanoparticles of Cu_2O. *Europhys. Lett.* **D. Chakravorty,** *52*, 468-473.

19. Bi, F.; Ehsan, M. F.; Liu, W.; He, T., Visible-Light Photocatalytic Conversion of Carbon Dioxide into Methane Using Cu2O/TiO2Hollow Nanospheres. *Chin. J. Chem.* **2015,** *33* (1), 112-118.
20. Tamiolakis, I.; Papadas, I. T.; Spyridopoulos, K. C.; Armatas, G. S., Mesoporous Assembled Structures of Cu_2O and TiO_2 Nanoparticles for Highly Efficient Photocatalytic Hydrogen Generation from Water. *RSC Advances* **2016,** *6* (60), 54848-54855.
21. Polliotto, V.; Livraghi, S.; Krukowska, A.; Dozzi, M. V.; Zaleska-Medynska, A.; Selli, E.; Giamello, E., Copper-Modified TiO2 and ZrTiO4: Cu Oxidation State Evolution during Photocatalytic Hydrogen Production. *ACS Appl Mater Interfaces* **2018,** *10* (33), 27745-27756.
22. Cerrato, E.; Gionco, C.; Berruti, I.; Sordello, F.; Calza, P.; Paganini, M. C., Rare earth ions doped ZnO: Synthesis, characterization and preliminary photoactivity assessment. *Journal of Solid State Chemistry* **2018,** *264*, 42-47.
23. Cerrato, E.; Zickler, G. A.; Paganini, M. C., The role of Yb doped ZnO in the charge transfer process and stabilization. *Journal of Alloys and Compounds* **2020,** *816*, 152555.
24. Evans, S. M.; Giles, N. C.; Halliburton, L. E.; Kappers, L. A., Further characterization of oxygen vacancies and zinc vacancies in electron-irradiated ZnO. *Journal of Applied Physics* **2008,** *103* (4), 043710.
25. R. Buchheit; F. Acosta-Humanez; Almanza, O., Structural, EPR and Optical Studies on Cu-doped ZnO Nanoparticles Synthetized by the Sol-Gel Method at Different Calcination Temperatures *Rev. Cub. Fis.* **2016,** *33*, 4-12.
26. Elilarassi, R.; Chandrasekaran, G., Structural, optical and electron paramagnetic resonance studies on Cu-doped ZnO nanoparticles synthesized using a novel auto-combustion method. *Frontiers of Materials Science* **2013,** *7* (2), 196-201.
27. Sreethawong, T.; Yoshikawa, S., Enhanced photocatalytic hydrogen evolution over Pt supported on mesoporous TiO2TiO2 prepared by single-step sol–gel process with surfactant template. *International Journal of Hydrogen Energy* **2006,** *31* (6), 786-796.
28. Parveen, F.; Sannakki, B.; Mandke, M. V.; Pathan, H. M., Copper nanoparticles: Synthesis methods and its light harvesting performance. *Solar Energy Materials and Solar Cells* **2016,** *144*, 371-382.